

---

# Controlled generation of rotating vector beams in quasi-isotropic laser

Krasnoshchekov Ye. A., Yaparov V. V. and Taranenko V. B.

International Center “Institute of Applied Optics” of the National Academy of Sciences of Ukraine, Kyiv, Ukraine, e-mail: evgen\_krasnoshokov@meta.ua

**Received:** 30.11.2018

**Abstract.** We investigate numerically polarization dynamics of a quasi-isotropic laser with weak loss anisotropy and a moderate Fresnel number, which involves competition of orthogonally polarized transverse modes. We demonstrate spontaneous formation of the first-, second- and third-order vector modes that reveal polarization structure of full Poincaré beams and show controllable transformations of the laser-field polarization structure and changes in its rotational dynamics.

**Keywords:** quasi-isotropic lasers, vector laser dynamics, full Poincaré beams

**PACS:** 47.54.-r, 42.60.Jf, 42.25.Ja

**UDC:** 621.373.826+535.41

## 1. Introduction

It is known that a polarization-isotropic laser having cylindrical symmetry can emit the vector beams with inhomogeneous polarization structures covering the entire surface of the Poincaré sphere [1]. In practice, however, some loss anisotropy is always present in a laser cavity. It breaks the cylindrical symmetry and creates a preference for a particular polarization state (usually a linear polarization). Nonetheless, if the loss anisotropy is weak enough, such a quasi-isotropic laser can sustain oscillations of the two polarization modes, one with a preferable polarization and another with the polarization orthogonal to it [2]. When the coupling between the polarization modes is weak and some phase anisotropy is also involved, such two-polarization lasers can operate as dual-frequency devices and reveal a number of useful features for such applications as, e.g., vibrometry [3], optical microwave generation [4] and lidars [5]. Note that polarization dynamics of the quasi-isotropic lasers can be very complicated [6, 7], being dependent on the strength of coupling between the orthogonal polarization modes.

In the present work we extend the studies of formation of the vector beams to the case of quasi-isotropic laser with weak loss anisotropy and strong coupling between the orthogonally polarized modes. Using a numerical solution of the two coupled laser equations, we demonstrate spontaneous formation of the vector beams with polarization structures of the full Poincaré beams, which represent polarization-spatial modes that carry nonzero angular momentums [8, 9]. We find the stability regions for the zero- and higher-order vector modes as functions of the laser aperture and the loss anisotropy. Controllable transformations of the polarization structure of the laser field and changes in its rotational dynamics are demonstrated, too.

## 2. Vector laser model

We consider a vector model for a single-longitudinal-mode high-quality laser with weak anisotropic losses. A laser cavity is suggested to be composed of two plane parallel mirrors and to contain polarization-isotropic-gain, dichroic and birefringent plates. This creates variable

anisotropic loss and phase. A circular diaphragm with the radius  $r$  controls the Fresnel number of the cavity  $N_F = r^2/\lambda L$  (with  $\lambda$  being the laser wavelength and  $L$  the resonator length) and allows selecting the transverse modes. Such a laser sustains oscillations of the two orthogonally polarized modes, thus forming a spatially structured vector laser field. Since the laser quality is high and the intra-cavity loss is low, the transverse structure of the vector laser field changes only slightly when the light propagates between the flat mirrors of the cavity. In this case the complex (slowly varying in space and time) amplitude of the vector laser field can be averaged over the longitudinal coordinate and represented by the following two transversely structured amplitudes of orthogonally polarized vectors:

$$\vec{E}(x, y, t) = \vec{e}_1 E_1(x, y, t) + \vec{e}_2 E_2(x, y, t), \quad (1)$$

where  $\vec{e}_1, \vec{e}_2$  are the unit vectors for the linear ( $\vec{e}_1 = \vec{e}_x, \vec{e}_2 = \vec{e}_y$ ) or circular ( $\vec{e}_1 = \vec{e}_+, \vec{e}_2 = \vec{e}_-$ ) polarization bases. Note that the orthogonal components in Eq. (1) can have different frequencies depending on the phase anisotropy of the cavity and different spatial structures depending on the cavity aperture.

The relaxation times for the population inversion and the polarization of gain medium are assumed to be negligibly small if compared with the lifetime of the intra-cavity light-field relaxation (a case of a so-called class-A laser). To calculate the evolution of the transversely structured vector laser-field envelope (in the form of Eq. (1)), which is formed inside the laser cavity with a saturable gain  $G(I)$ , we use two coupled laser equations taken in the form of the following system of extended Ginsburg–Landau equations:

$$\partial E_{1,2}/\partial t = (d_{Re} + id_{Im}) \nabla_{\perp}^2 E_{1,2} + [G(I) + i\theta_{1,2} - \eta_{1,2}] E_{1,2}. \quad (2)$$

Here  $t$  is the time measured in the units of field-decay time for the empty cavity,  $d_{Re}$  and  $d_{Im}$  are respectively the effective diffusion and diffraction coefficients,  $\nabla_{\perp}^2 = \partial^2/\partial x^2 + \partial^2/\partial y^2$  denotes the transverse Laplace operator,  $I = |E_1|^2 + |E_2|^2$  the total intra-cavity light intensity normalized to the saturated intensity  $I_S$  (so that the gain is reduced to half of its unsaturated value at  $I_S$ ),  $G(I) = g_0/(1+I)$  implies the saturable gain (with  $g_0$  denoting the unsaturated gain),  $\theta_{1,2}$  are detunings for the orthogonal polarization modes created by a birefringent element that produces the phase anisotropy, and  $\eta_{1,2}$  are the linear loss coefficients for the orthogonal polarization modes, which reveal the loss anisotropy imposed by a dichroic element.

The transverse coordinates  $x$  and  $y$  are measured in the units of the Fresnel-zone width,  $w_F = [L\lambda/4\pi(1-R)]^{1/2}$ , where  $R$  is the product of reflectivity coefficients of the mirrors. Eq. (2) describes interaction of the orthogonally polarized components,  $E_1(x, y, t)$  and  $E_2(x, y, t)$ , of the optical field via the effect of cross-saturation of the gain medium. We assume that the gain medium is spatially homogeneous and its coefficients of self-saturation and cross-saturation are equal to unity, which implies strong competition between the orthogonally polarized modes.

### 3. Numerical simulations

To find the transverse polarization structure of the vector laser field and the intensity/phase structure of each of its polarization components, we solve Eq. (2) numerically, using a standard Fourier split-step method. The transverse boundary conditions are defined at the edge of the

circular diaphragm, which is modelled by the  $\eta_{1,2}$  parameters in the form of six-order super-Gaussian function of the radius  $r$ . The initial conditions are specified as a random noise, which starts formation of a transversely structured vector laser field.

We limit our studies to searching for those vector laser modes only that reveal axially symmetric intensity profiles. Such the structures are formed spontaneously at moderate Fresnel numbers of the resonator ( $1 < N_F < 10$ ). As explained below, the vector modes  $\vec{V}_r^l = \vec{e}_1 LG_0^l + \vec{e}_2 LG_r^0$  are reduced to mutually trapped, orthogonally polarized a spiral-phase Laguerre–Gauss mode  $LG_0^l$  (with  $l$  denoting the azimuthal index) and a radial mode  $LG_r^0$  (with  $r$  being the radial index). On the contrary, we will deal with the irregular structures with polarization topological defects [10], whenever the Fresnel number of the cavity becomes large enough ( $N_F > 10$ ).

For numerical calculations, the following normalized parameters entering Eq. (2) have been used:  $g_0 = 2$ ,  $d_{re} = 2 \times 10^{-4}$ , and  $d_{im} = 2 \times 10^{-3}$ . The transverse structure of the vector laser fields is examined depending on the cavity Fresnel number, as well as the loss and phase anisotropies.

#### 4. Results and discussion

As mentioned above, we study the effects of loss ( $\eta_1 \neq \eta_2$ ) and phase ( $\theta_1 \neq \theta_2$ ) anisotropies on the effect of spontaneous formation and the polarization dynamics of the vector modes in the quasi-isotropic laser with variable diaphragm (i.e., a changing  $N_F$  parameter). We start with a zero-order vector mode, which involves only polarization dynamics. Then we consider a competition of polarization and spatial fields that leads to formation of higher-order vector modes.

##### 4.1. Zero-order vector mode

First we study the polarization structure and its dynamics for the laser with a small-size intra-cavity diaphragm, which corresponds to the case of  $N_F \approx 1$ . Then only the zero-order vector mode  $\vec{V}_0^0 = \vec{e}_1 LG_0^0 + \vec{e}_2 LG_0^0$  is allowed to oscillate, for which the orthogonally polarized components are spatially identical and completely overlapped. Under this condition, the polarization modes interact with the same volume of the gain material and none of them acquires advantage over the other.

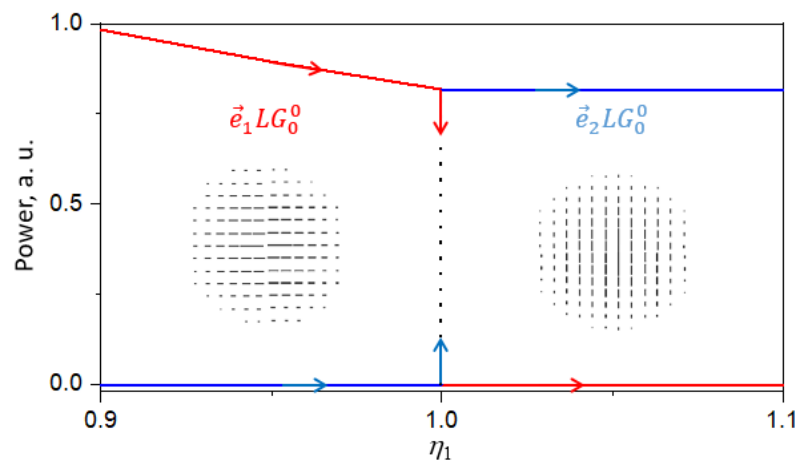


**Fig. 1.** Structure of orthogonal polarization components  $\vec{e}_1 LG_0^0$  and  $\vec{e}_2 LG_0^0$ , and their powers  $P_1$  (red) and  $P_2$  (blue) versus linear loss coefficient  $\eta_1$ , as calculated at  $N_F \approx 1$  and  $\eta_2 = 1$ .

When the intra-cavity loss anisotropy is involved, one of the polarization components acquires advantage over the other, so that the powers of the orthogonally polarized components ( $P_{1,2} = \int |E_{1,2}|^2 ds$ , with  $S$  being the diaphragm area) become different. Having solved Eq. (2) with the parameters specified above, we obtain a switching regime of the laser oscillation: the lasing occurs either in  $\vec{e}_1 LG_0^0$  or in  $\vec{e}_2 LG_0^0$  mode, depending on the sign of the loss anisotropy ( $\eta_1 - \eta_2$ ). The polarization of the laser field switches abruptly between these orthogonal polarization modes when  $\eta_1 = \eta_2$  (see Fig. 1). If the laser emission occurs at  $\eta_1 = \eta_2$  and  $\theta_1 = \theta_2$ , the steady-state solutions of Eq. (2) are characterized by a homogeneous polarization which can correspond to any state, i.e. to an arbitrary point of the Poincaré sphere.

When the phase anisotropy is present in the laser cavity and we have  $\eta_1 = \eta_2$  (i.e., the orthogonal polarization fields have different detunings,  $\theta_1 \neq \theta_2$ ), the laser goes into the dynamic regime of polarization oscillations, although the field remains transversely uniform at each time instant. This is a well-known dual-frequency operation regime of the anisotropic laser [11, 12]. As expected for the above case, the polarization-oscillation frequency is proportional to  $(\theta_1 - \theta_2)$ .

#### 4.2. First-order vector modes

For the case of  $N_F \approx 3 \dots 5$ , steady-state solutions of Eq. (2) have the form of rotating polarization structures of the two axially symmetrical first-order vector modes,  $\vec{V}_0^{\pm 1} = \vec{e}_1 LG_0^{\pm 1} + \vec{e}_2 LG_0^0$  (Fig. 2) and  $\vec{V}_1^{\pm 1} = \vec{e}_1 LG_1^{\pm 1} + \vec{e}_2 LG_1^0$  (Fig. 3). They represent mutually trapped and orthogonally polarized transverse modes with different azimuthal and radial indices. These polarization-spatial modes are formed spontaneously from the random noise and, therefore, the probabilities of forming the structures with the azimuthal index equal to either +1 or -1 amount to 50%. Simultaneous

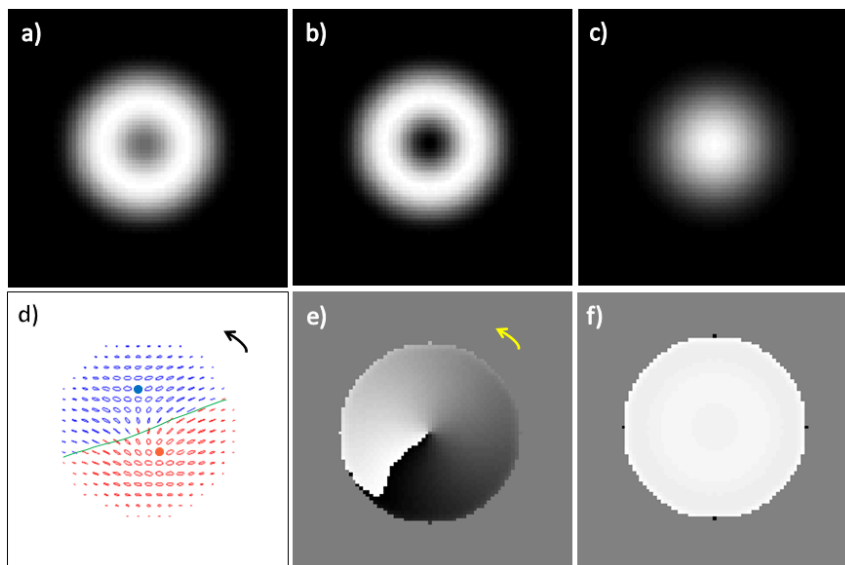


**Fig. 2.** Structure of first-order vector mode  $\vec{V}_0^{-1}$  calculated at  $N_F \approx 3$ ,  $\theta_2 - \theta_1 = 0$  and  $\eta_1 - \eta_2 = -0.03$ : transverse distributions of total intensity (a), map of polarization (polarization ellipses) in the linear polarization basis (d), and intensity (b)/(c) and instant phase (e)/(f) for the mutually trapped transverse mode  $LG_0^{-1}/LG_0^0$ . Red and blue ellipses denote respectively left-handed and right-handed polarization states. C+ and C- points are labelled with blue and red circles, respectively. Domains of left-handed (red) and right-handed (blue) polarization states are separated by L-lines (green). Arrows indicate rotation directions.

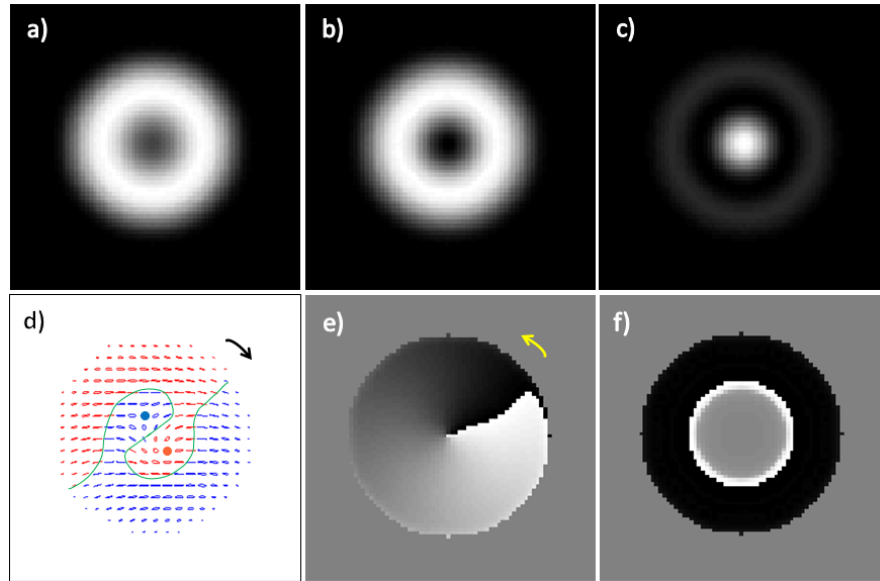


**Fig. 3.** Structure of vector mode  $\vec{V}_1^{-1}$  calculated at  $N_F \approx 5$ ,  $\theta_2 - \theta_1 = 0$  and  $\eta_1 - \eta_2 = -0.03$ . Notations are the same as in Fig. 2.

polarization and spatial competitions lead to the formation of complementary vector spatial structures, with the first-order azimuthal mode  $LG_0^{\pm 1}$  in one polarization state and the zero-order  $LG_0^0$  (or the first-order  $LG_1^0$ ) radial mode in the orthogonal polarization state. The polarization structures of the vector modes  $\vec{V}_0^{\pm 1}$  and  $\vec{V}_1^{\pm 1}$  are the same, which corresponds to the rotating full Poincaré beams of the types I and II of an ideally isotropic laser [1]. However, in the case of laser with the phase anisotropy, one can vary the optical length of the cavity separately for each of the polarization components and, thereby, change the frequency difference between the orthogonal transverse modes. This allows for controlling the value and the direction of rotational speed of the vector modes.

Beating of the orthogonal transverse modes that oscillate at different frequencies leads to rotation of the total polarization structure with the constant angular speed, even in the ideal isotropic case ( $\theta_2 - \theta_1 = 0$  and  $\eta_1 - \eta_2 = 0$ ). The rotational speed of the  $\vec{V}_0^{\pm 1}$  mode becomes zero whenever we have  $\theta_2 - \theta_1 = -0.42$  and  $\eta_1 - \eta_2 = 0$ . When  $\theta_2 - \theta_1 < -0.42$ , the direction of the polarization-structure rotation is opposite to that of the phase structure of the azimuthal component, and vice versa in the case of  $\theta_2 - \theta_1 > -0.42$ . The point of zero angular velocity for the polarization structure of the  $\vec{V}_1^{\pm 1}$  mode is  $\theta_2 - \theta_1 = 0.51$ . Note that these rotational transformations occur at a fixed azimuthal index of the vector modes.

The first-order vector modes  $\vec{V}_0^{\pm 1}$  and  $\vec{V}_1^{\pm 1}$  can be formed in the laser at the same Fresnel number of the cavity though at different loss anisotropies. Fig. 4 shows stability ranges (marked as Roman numerals) for these modes formed at  $N_F \approx 3$ , depending on the linear loss coefficient  $\eta_1$  and at  $\eta_2 = 1$ . In the zone I, the power  $P_1$  of the first component, which has the structure of the  $LG_0^{\pm 1}$  mode, takes all the laser gain and does not leave any power for the second polarization

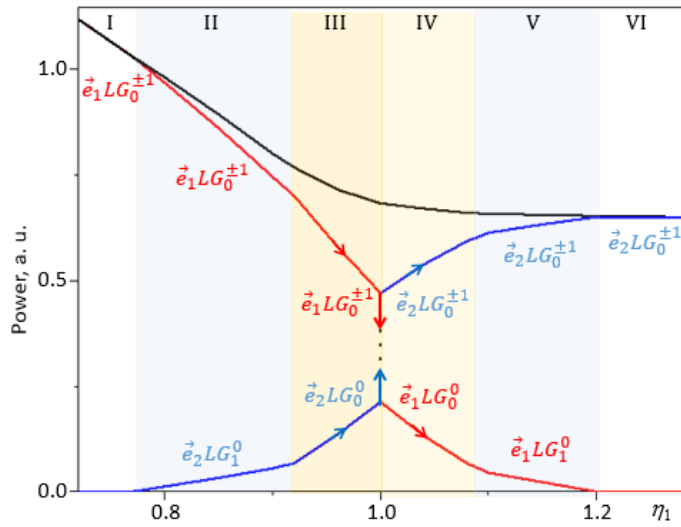


**Fig. 4.** Structure of orthogonally polarized mode components  $\vec{e}_1 LG_r^l$  (red) and  $\vec{e}_2 LG_r^l$  (blue), as well as their powers  $P_1$  (red curves) and  $P_2$  (blue curves) and the total power (black curve) versus linear loss coefficient  $\eta_1$ , as calculated at  $\eta_2 = 1$  and  $N_F \approx 3$ . Stability zones for polarization-spatial modes are marked by Roman numerals (see the text).

component. Therefore, the zone I represents a zone of scalar pattern where no vector-mode structures  $\vec{V}_r^l$  can exist. In the zone II, a vector mode  $\vec{V}_1^{\pm 1} = \vec{e}_1 LG_0^{\pm 1} + \vec{e}_2 LG_1^0$  with a vortex in the first component can be spontaneously formed (see Fig. 3). The vector mode  $\vec{V}_0^{\pm 1} = \vec{e}_1 LG_0^{\pm 1} + \vec{e}_2 LG_0^0$  with a vortex in the first component becomes stable in the zone III (see Fig. 2). The structural transition  $\vec{V}_1^{\pm 1} \rightarrow \vec{V}_0^{\pm 1}$  occurring between the zones II and III is accompanied by a dynamical transformation: the polarization structures of the vector modes  $\vec{V}_1^{\pm 1}$  and  $\vec{V}_0^{\pm 1}$  rotate in the opposite directions, provided that they have the same sign of the azimuthal index. The zone IV corresponds to the  $\vec{V}_0^{\pm 1}$  vector mode with a vortex in the second component, whereas the vector mode  $\vec{V}_1^{\pm 1}$  with a vortex in the second component is spontaneously formed in the zone V. Finally, the zone VI is a scalar-pattern zone of the second polarization component.

### 4.3. Second-order vector modes

As seen from Fig. 5, the second-order vector modes  $\vec{V}_0^{\pm 2} = \vec{e}_1 LG_0^{\pm 2} + \vec{e}_2 LG_0^0$  are spontaneously formed with increasing Fresnel number. They correspond to a non-separable, mutually trapped and orthogonally polarized zero-order radial mode and a spiral-phase mode with  $l = \pm 2$ . Note that the latter is unstable in the scalar case.

The second-order vector modes reveal the polarization structures of the full Poincaré beams, with polarization topological defects present. These are two L lines of linearly polarized states (green lines in Fig. 5) which separate the domains of opposite handedness, as well as two pairs of C point defects (i.e., the points of circular polarizations). A pair of C+ defects (blue) is surrounded by a pattern of ellipses having a ‘star’ morphology, with a tree radial direction of the ellipses’ major axes. There is also a pair of C– defects (red) having a ‘lemon’ morphology, with single radial directions of the major axes [13].

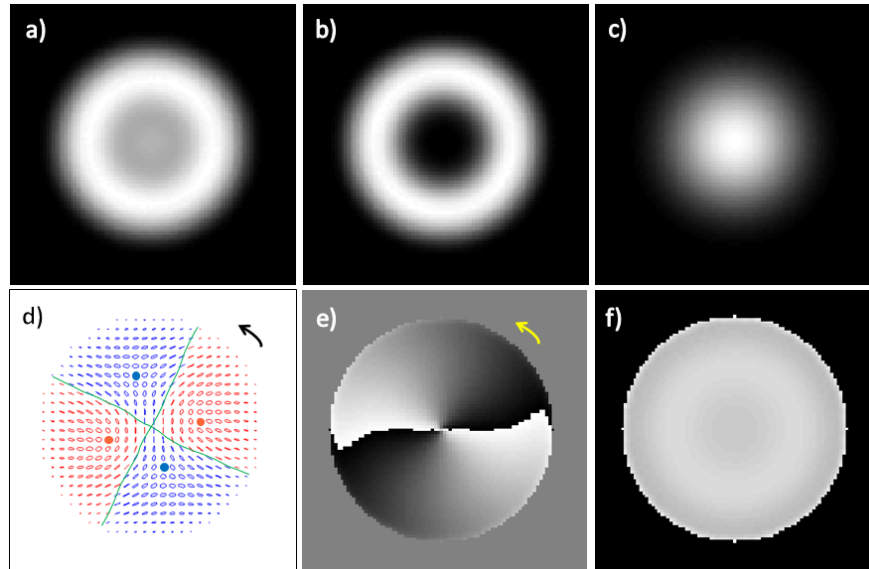


**Fig. 5.** Structure of vector mode  $\vec{V}_0^{-2}$  calculated at  $N_F \approx 6$ ,  $\theta_2 - \theta_1 = 0$  and  $\eta_1 - \eta_2 = -0.03$ . Notations are the same as in Fig. 2.

Fig. 6 displays dependence of the powers  $P_1$  and  $P_2$  of the both polarization components on the linear loss coefficient  $\eta_1$ , as obtained at  $\eta_2 = 1$  and  $N_F \approx 6$ . The ‘zonal structure’ shown in Fig. 6 is like that appearing in Fig. 4, except for the second and penultimate zones. These are the zones of irregular vector patterns where the axially symmetric vector modes cannot exist. There are two zones of stability of the  $\vec{V}_0^{\pm 2}$  mode in the region  $\eta_1 \in [0.82; 1.12]$ . As evident from Fig. 6, they are separated by the isotropy point  $\eta_1 = \eta_2 = 1$ . Two structural transformations occur at this point: we have  $LG_0^{\pm 2} \rightarrow LG_0^0$  for the first polarization component and  $LG_0^0 \rightarrow LG_0^{\pm 2}$  for the second polarization component.

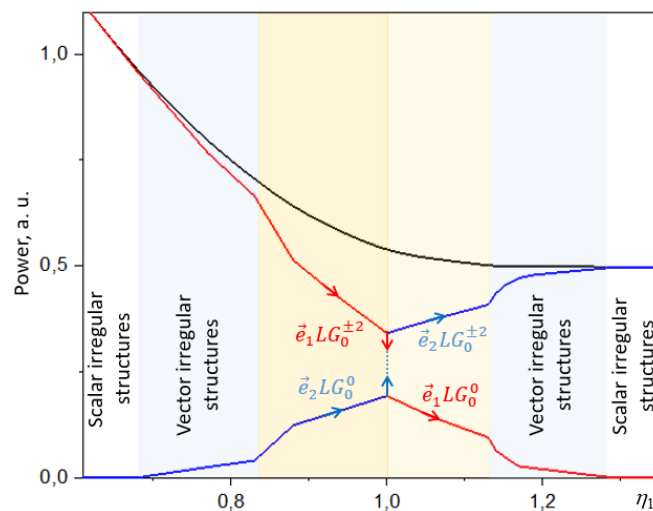


**Fig. 6.** Powers  $P_1$  (red) and  $P_2$  (blue) of the polarization components, and the total power (black) versus linear loss coefficient  $\eta_1$ , as calculated at  $\eta_2 = 1$  and  $N_F \approx 6$ .

#### 4.4. Third-order vector modes

When the Fresnel number increases up to  $N_F \approx 7$ , we find stable third-order vector structures  $\vec{V}_0^{\pm 3} = \vec{e}_1 LG_0^{\pm 3} + \vec{e}_2 LG_0^0$  (see Fig. 7). The third-order spiral-phase modes  $LG_0^{\pm 3}$ , which are unstable in a scalar laser with strong loss anisotropy, become stable in the quasi-isotropic laser due to a stabilizing role of the zero-order radial mode  $LG_0^0$ . The vector modes acquire the polarization structures typical for the full Poincaré beams. They rotate around the beam axis in a controllable manner due to changing phase anisotropy. These structures also contain the polarization topological defects, three L lines of the linearly polarized states (see green lines in Fig. 7) and six C point defects. Three C+ defects (blue) are surrounded by a pattern of ellipses having a ‘star’ morphology, whereas three C– defects are surrounded by a pattern of ellipses with ‘lemon’ morphology. The zonal structure obtained for the laser with this Fresnel number is similar to that found for the laser with  $N_F \approx 6$  (see Fig. 6). At the isotropy point, structural transformations  $LG_0^{\pm 3} \rightarrow LG_0^0$  and  $LG_0^0 \rightarrow LG_0^{\pm 3}$  occur respectively for the first and second polarization components.

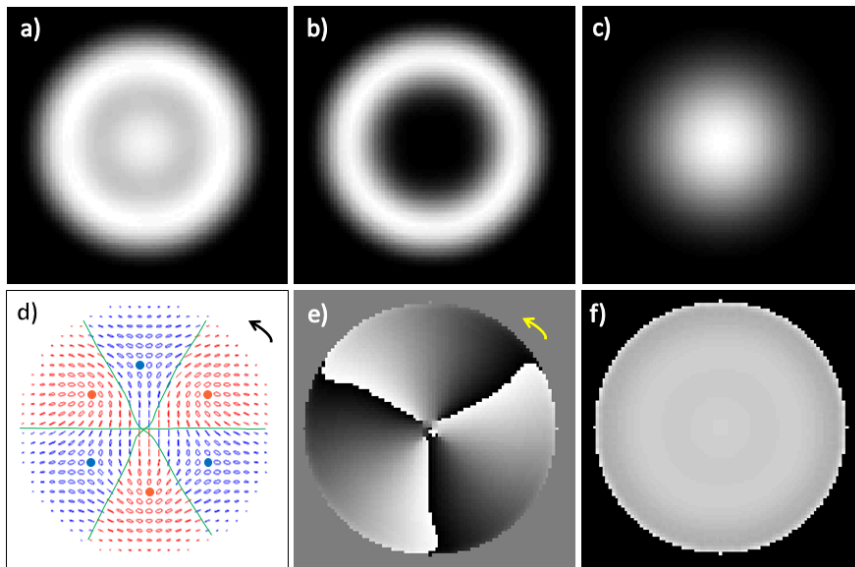


**Fig. 7.** Structure of vector mode  $\vec{V}_0^{-3}$  calculated at  $N_F \approx 7$ ,  $\theta_2 - \theta_1 = 0$  and  $\eta_1 - \eta_2 = -0.03$ . Notations are the same as in Fig. 2.

#### 5. Conclusion

We have studied the effects of spontaneous formation of rotating vector beams in the single-longitudinal-mode quasi-isotropic laser with weak loss anisotropy and a moderate Fresnel number of the cavity. Our numerical simulations show that the vector laser modes are formed from a random noise under conditions when different polarization and spatial fields compete with each other. As a result, pairs of mutually trapped, orthogonally polarized azimuthal and radial Laguerre–Gauss modes of different orders are formed. They have axially symmetric profiles of the total intensity and spatially inhomogeneous polarization structures of the full Poincaré beams, which rotate around the beam axis with constant speeds. We have demonstrated that one can control both the magnitude and the direction of angular speed of the polarization structure of these vector modes, when varying the phase anisotropy of the laser cavity.

**References**

1. Krasnoshchekov Ye, Yaparov V and Taranenko V, 2017. Rotating full Poincaré beams. Ukr. J. Phys. Opt. **18**: 1–8.
2. Abraham N, Matlin M and Gioggia R, 1996. Polarization stability and dynamics in a model for a polarization-isotropic laser that goes beyond third-order Lamb theory. Phys. Rev. A. **53**: 3514–3528.
3. Czarske J and Mueller H. 1995. Birefringent Nd:YAG microchip laser used in heterodyne vibrometry. Opt. Commun. **114**: 223–229.
4. Brunel M, Bretenaker F and Le Floch A. 1997. Tunable optical microwave source using spatially resolved laser eigenstates. Opt. Lett. **22**: 384–386.
5. He C. and Killinger D. 1994. Dual-polarization modes and self-heterodyne noise in a single-frequency 2.1- $\mu\text{m}$  microchip Ho, Tm:YAG laser. Opt. Lett. **19**: 396–398.
6. Zolotoverkh L and Lariontsev E, 2004. Bistability and chaos in an autonomous Nd: YAG laser with a weakly anisotropic resonator. Quant. Electron. **34**: 727–730.
7. Leyva I, Allaria E and Meucci R, 2003. Polarization and spatial competition in a transverse multimode CO<sub>2</sub> laser. Phys. Rev. A. **68**: 0538XX-1–8.
8. Beckley A, Brown T and Alonso M, 2010. Full Poincaré beams. Opt. Express. **18**: 10777–10785.
9. Wang L-G, 2012. Optical forces on submicron particles induced by full Poincaré beams. Opt. Express. **20**: 20814–20826.
10. Gil L, 1993. Vector order parameter for an unpolarized laser and its vectorial topological defects. Phys. Rev. Lett. **70**: 162–165.
11. Otsuka K, 1978. Oscillation properties of anisotropic lasers. IEEE J. Quant. Electron. **QE-14**: 49–55.
12. Dekker P and Dawes J, 1998. Pulsed output from a dual-polarization cw diode-pumped Nd:YAG laser. J Opt. Soc. Amer. B. **15**: 247–251.
13. Nye J. Natural focusing and fine structure of light: Caustics and wave dislocations. Bristol: IOP Publishing (1999).

---

Krasnoshchekov Ye. A., Yaparov V. V. and Taranenko V. B. 2019. Controlled generation of rotating vector beams in quasi-isotropic laser. Ukr.J.Phys.Opt. **20**: 1–9. doi: 10.3116/16091833/20/1/1/2019

***Анотація.** Досліджено динаміку поляризації світла квазі-ізотропного лазера зі слабкою анізотропією втрат і помірним числом Френеля, яка включає конкуренцію ортогонально поляризованих поперечних мод. Продемонстровано можливість спонтанного формування векторних мод першого, другого і третього порядків, які виявляють поляризаційну структуру т. зв. повних пучків Пуанкаре, керовані перетворення структури поляризації лазерного поля, а також зміни динаміки її обертання.*